Electronic Supporting Information

Synthesis and Structural Characterisation of Unprecedented Primary *N*-nitrosamines Coordinated to Iridium(IV)

Ana Foi, Florencia Di Salvo*, Fabio Doctorovich*, Cristián Huck-Iriart, José Martín Ramallo-López, Maximilian Dürr, Ivana Ivanović-Burmazović, Kathrin Stirnat, Simon Garbe and Axel Klein*

Contents

D. References

A Supplementary Tables

Table 1. Selected UV/Vis absorptions recorded during anodic oxidation of $[\mathbf{1}]^{2-}$ and $[\mathbf{2}]^{2-}$.[a]

Species	λ / nm (ε / M^{-1} cm^{-1})
$[\mathbf{1}]^{2-}$	244(1804), 334(498)
$[\mathbf{1}]^{\bullet-}$	254(3075), ~350 and 430 very low intensity, 544 (541)
$[\mathbf{2}]^{2-}$	244(2779), 328 (1047)
$[\mathbf{2}]^{\bullet-}$	253(5371), ~350 and 430 very low intensity, 544 (1426)
	For comparison
$[IrCl_6]^{2-}$ [b]	232 (15050), 306 (510), 434 (2500), 488 (3500), 588 (100)
$[IrCl_6]^{3-}$ [c]	- ……, 320 (60), 415 (70), 590 (10)

[a] Measured in DMSO/nBu$_4$NPF$_6$ at room temperature in an OTTLE cell

[b] Measured in H_2O, from ref. S1.

[c] Measured in aquat. 4M HCl, from ref. S2.

B Supplementary Figures

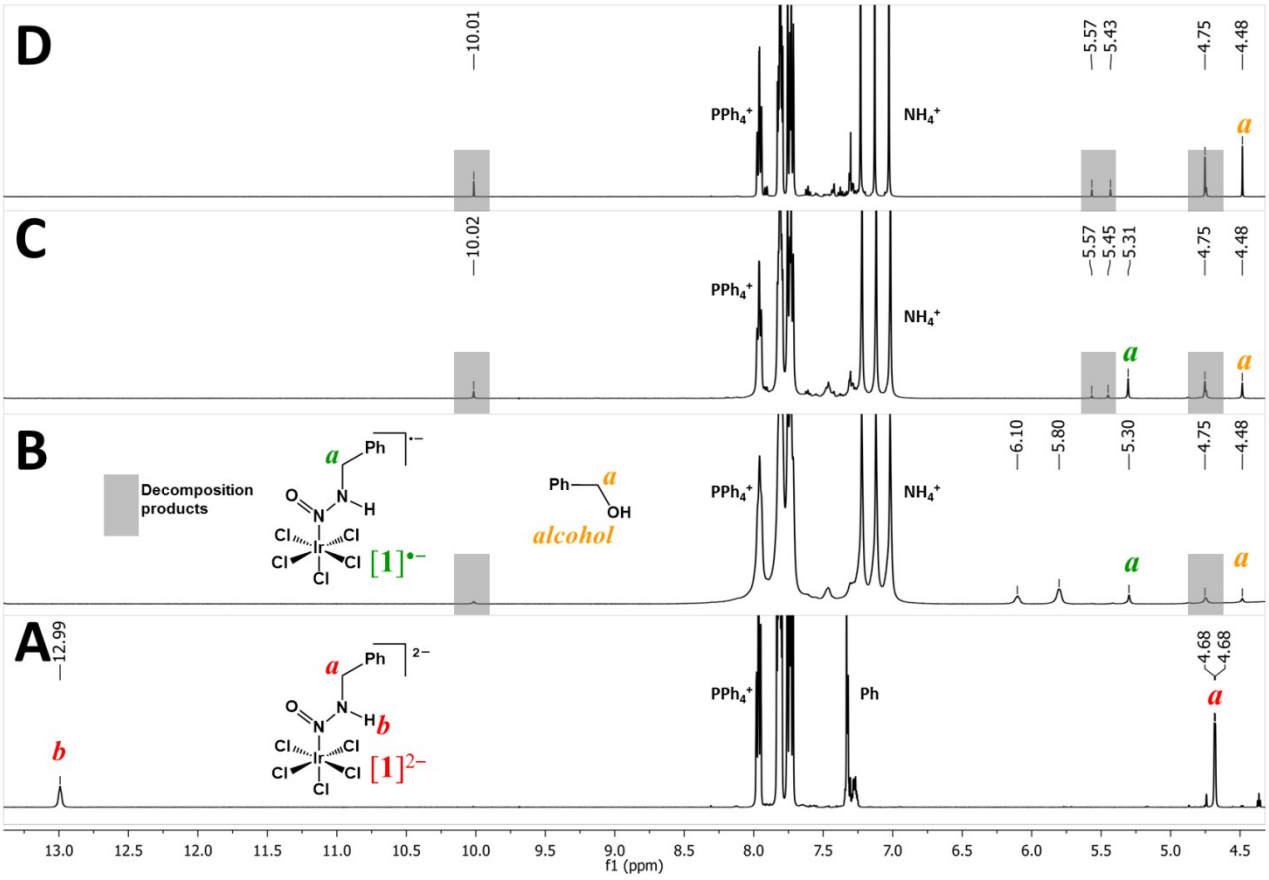

Figure S1. Oxidation of $(PPh_4)_2$[**1**] in DMSO-d^6 using $(NH_4)_2[Ce^{IV}(NO_3)_6]$, followed by ^{1}H NMR (500 MHz) spectroscopy. **A**: starting complex; **B**: spectrum recorded immediately after addition. Signals were broadened and $[\mathbf{1}]^-$ is observed at 5.3 ppm together with benzyl alcohol (4.5 ppm) and some unidentified (transient) decomposition products (marked in grey). **C**: spectrum recorded after 40 minutes. Some transient species disappeared, $[\mathbf{1}]^{\bullet-}$ is still observed, other decomposition products presumably benzaldehyde and benzoic acid appeared. **D**: spectrum recorded after 48 hours. Signals for $[\mathbf{1}]^-$ were not observed anymore, persistent signals are 4.5 (benzylic alcohol) 4.75, 5.45, 5.57 and 10.0 ppm.

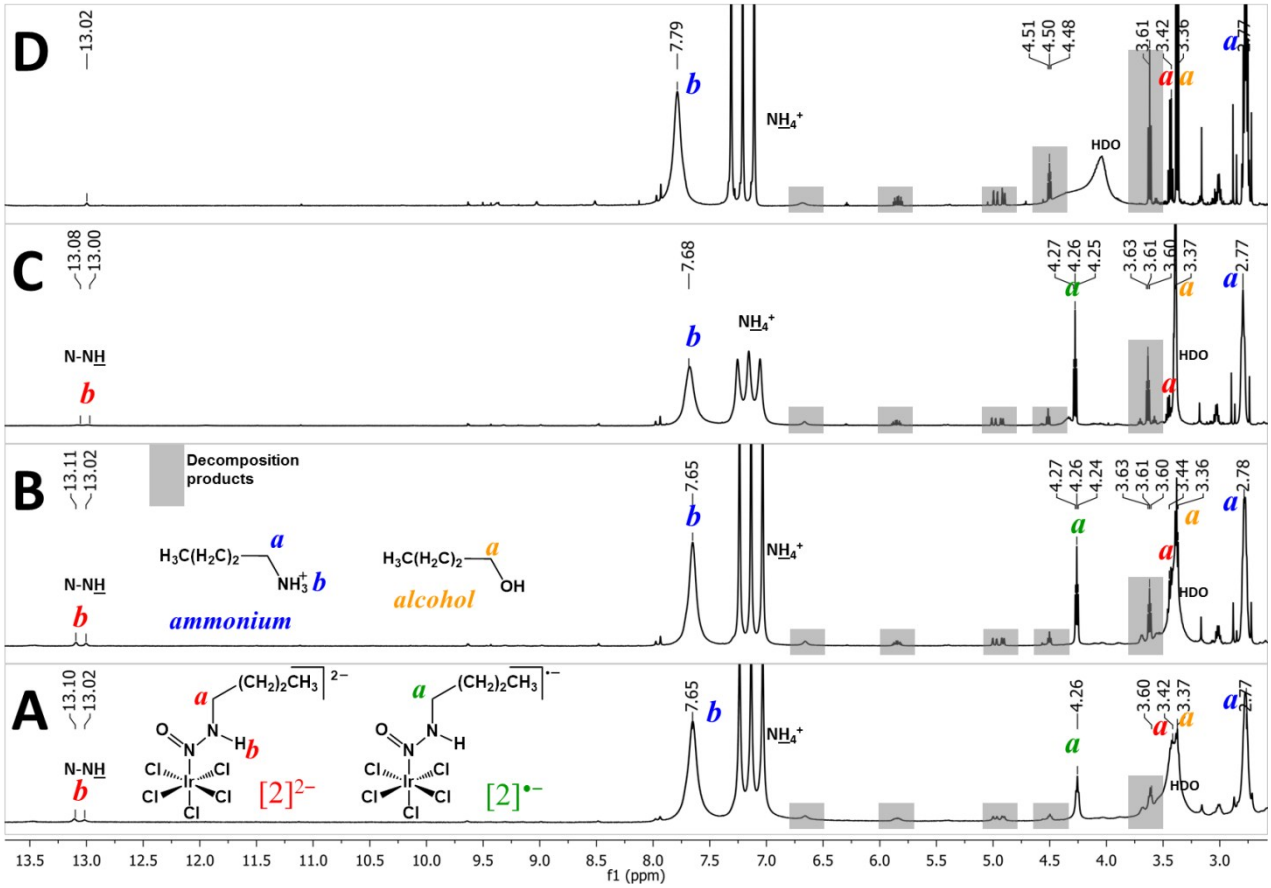

Figure S2. Oxidation of K(BuNH$_3$)[**2**] in DMSO using $(NH_4)_2[Ce^{IV}(NO_3)_6]$, followed by ^{1}H NMR (500 MHz) spectroscopy. **A**: spectrum recorded immediately after addition of the oxidant. Signals were broadened, a new species at 4.26 ppm is assigned to [**2**]$^{\bullet-}$, butyl alcohol is detected at 3.44 ppm, the ammonium $BuNH_3^+$ is observed at 2.78 ppm, other yet unknown decomposition products were highlighted in grey. **B**: spectrum recorded after 10 minutes. **C**: spectrum recorded after 30 minutes. [**2**]$^-$ can still be observed. D: Spectrum after 24 h shows [**2**]$^-$, the absence of [**2**]$^{\bullet-}$ and an increase of the alcohol and other decomposition products.

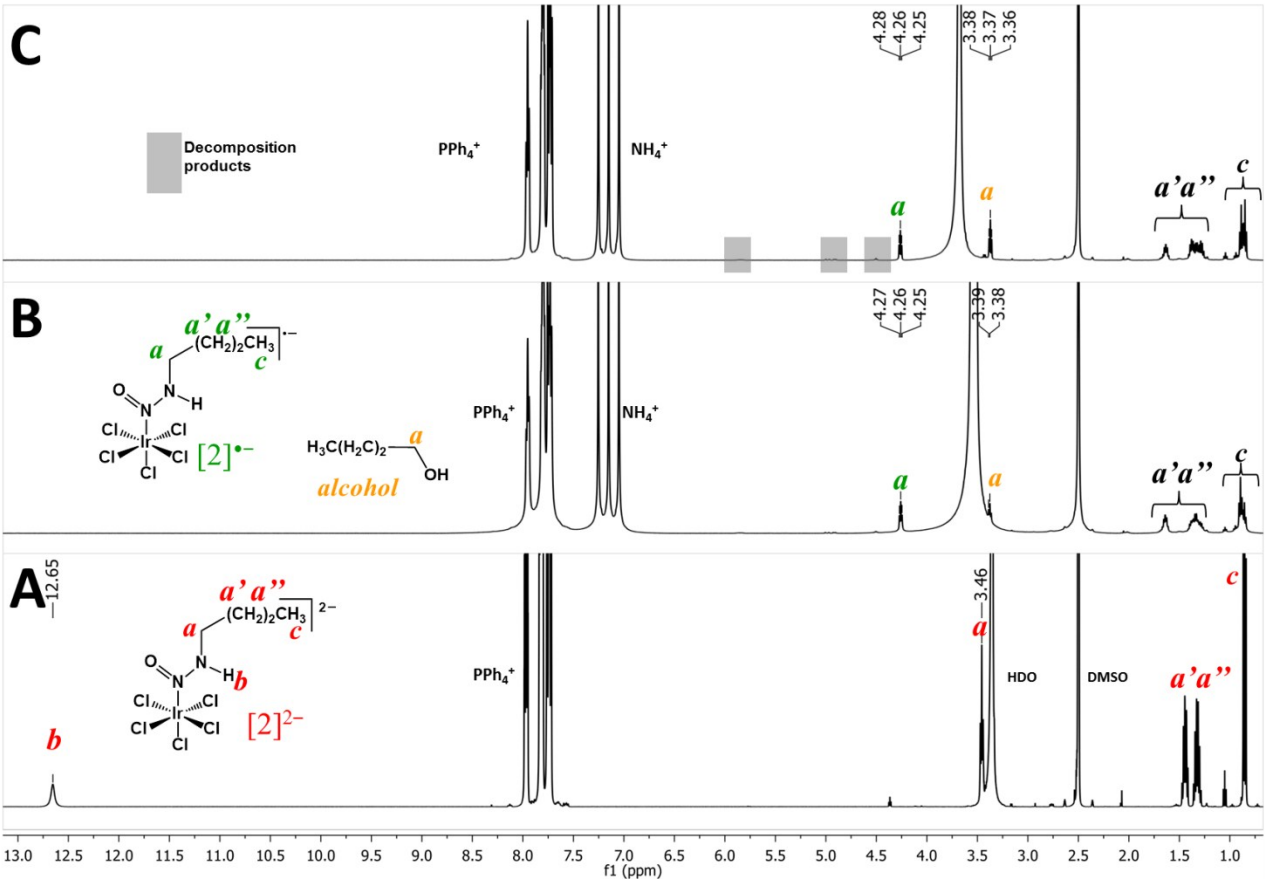

Figure S3. Oxidation of $(PPh_4)_2$[**2**] in DMSO-d^6 using $(NH_4)_2[Ce^{IV}(NO_3)_6]$, followed by ^{1}H NMR (500 MHz) spectroscopy. **A**: starting complex $[\mathbf{2}]^{2-}$; **B**: spectrum recorded immediately after addition of the oxidant. Signals were broadened signals, butyl alcohol is detected at 3.4 ppm and the new species at 4.26 ppm is assigned to $[\mathbf{2}]^{\bullet-}$. **C**: spectrum recorded after 60 minutes. Butyl alcohol and $[\mathbf{2}]^{\bullet-}$ are detected together with un-identified further decomposition products highlighted in grey.

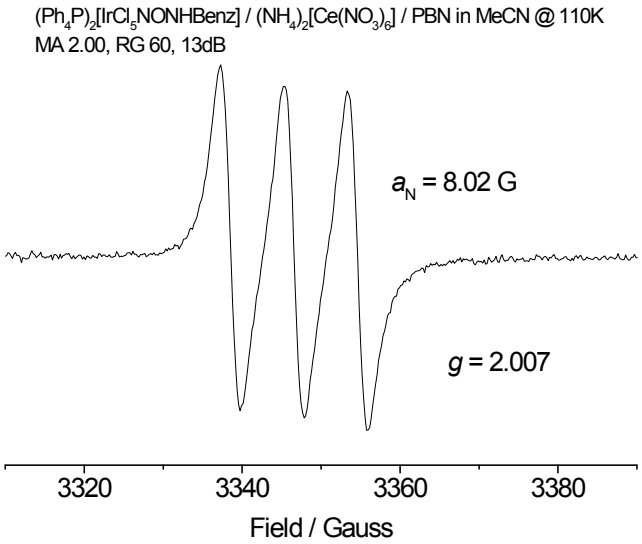

Figure S4. Oxidation of $(PPh_4)_2$[**2**] in MeCN using $(NH_4)_2[Ce^{IV}(NO_3)_6]$ in the presence of PBN (*N-tert.*-butyl-α-phenylnitrone). X-band EPR spectrum recorded at 110 K in glassy frozen solution after 15 min reaction time. The observed signal with a_N = 8.02 G does not represent the PBN-OH trap (a_N = 15.4 G, a_H = 2.7 G) but the oxidised product PhC(O)N(•O)^{t}Bu.[S3,S4]

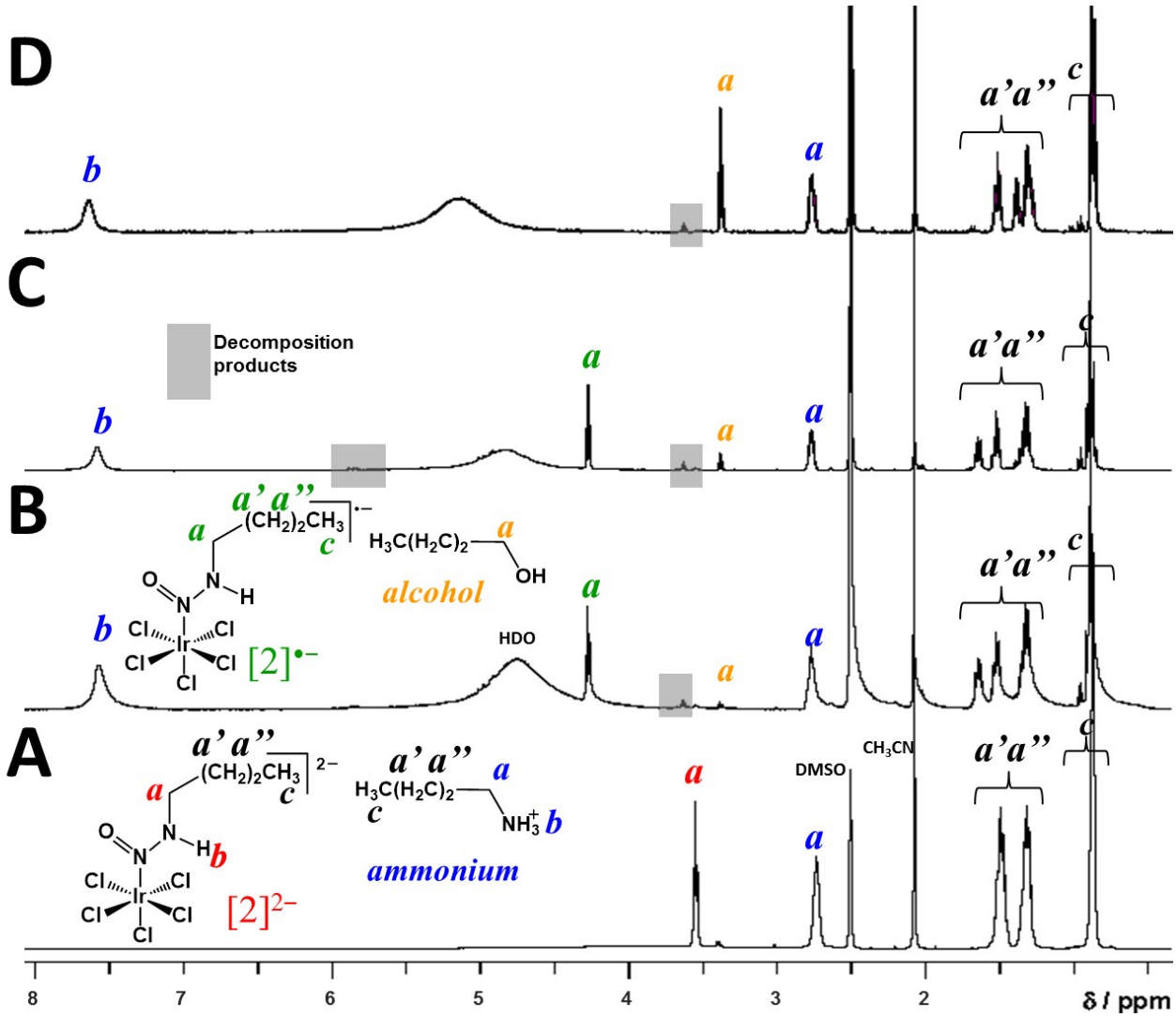

Figure S5. Decomposition of K($BuNH_3$)[**2**] in DMSO-d^6/TFA (trifluoroacetic acid) followed by ^1H NMR (500 MHz) spectroscopy. **A**: starting complex. **B**: spectrum recorded immediately after addition of 1 equivalent of TFA. The species observed at 4.31 ppm can be assigned to [**2**]$^{\bullet-}$; **C**: spectrum recorded after 45 min. **D**: spectrum recorded after 30 h. The strongest product signal comes from butyl alcohol at 3.5 ppm.

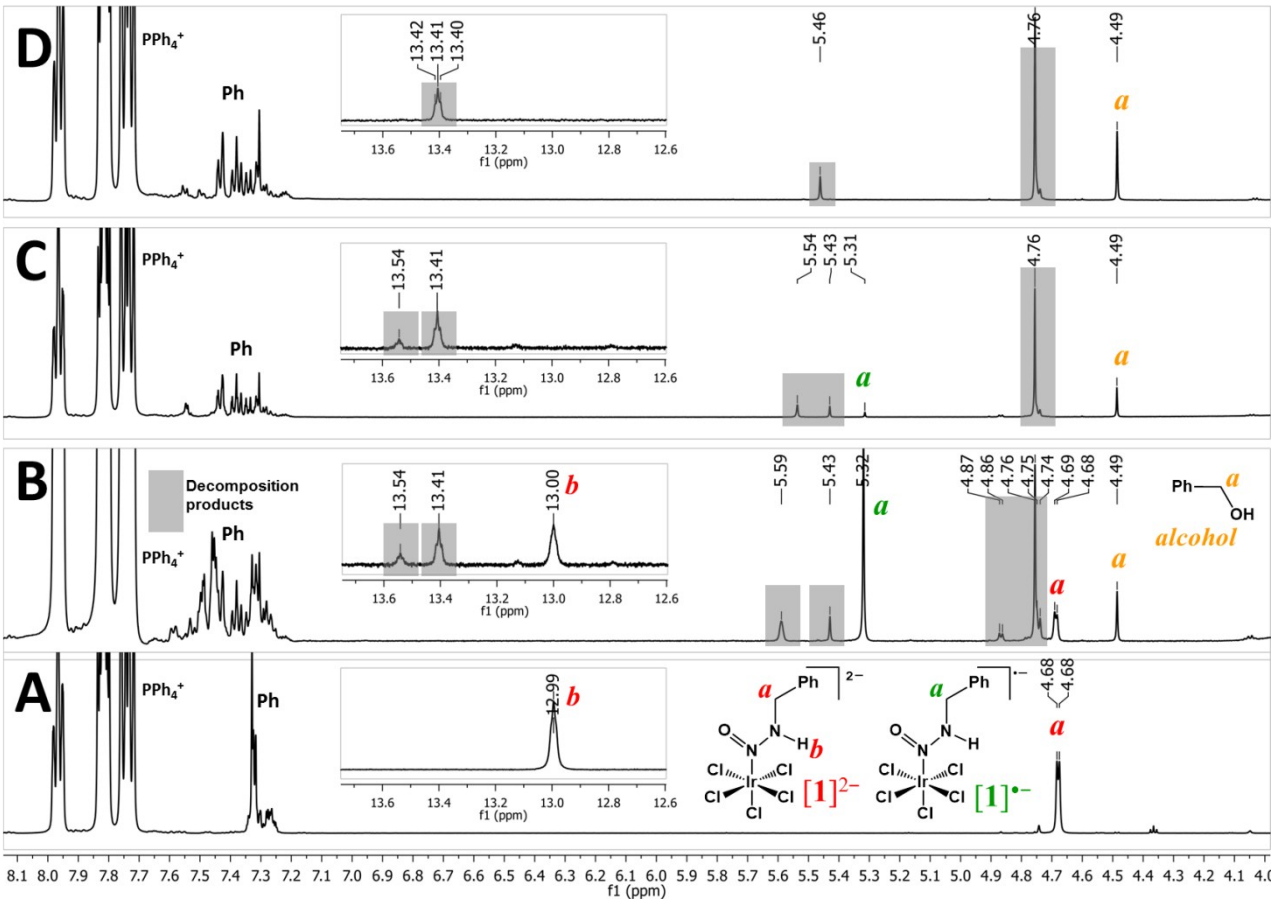

Figure S6. Decomposition of $(PPh_4)_2$[**1**] in DMSO-d^6/TFA (trifluoroacetic acid) followed by ^{1}H NMR (500 MHz) spectroscopy. **A**: starting complex. **B**: spectrum recorded immediately after addition of 1 equivalent of TFA. At 5.32 ppm a new species is detected which turns out to be [**1**]$^{\bullet-}$, at 4.49 ppm benzyl alcohol is detected, other yet un-identified decomposition products are highlighted in grey. **C**: spectrum recorded after 60 min. **D**: spectrum recorded after 96 h.

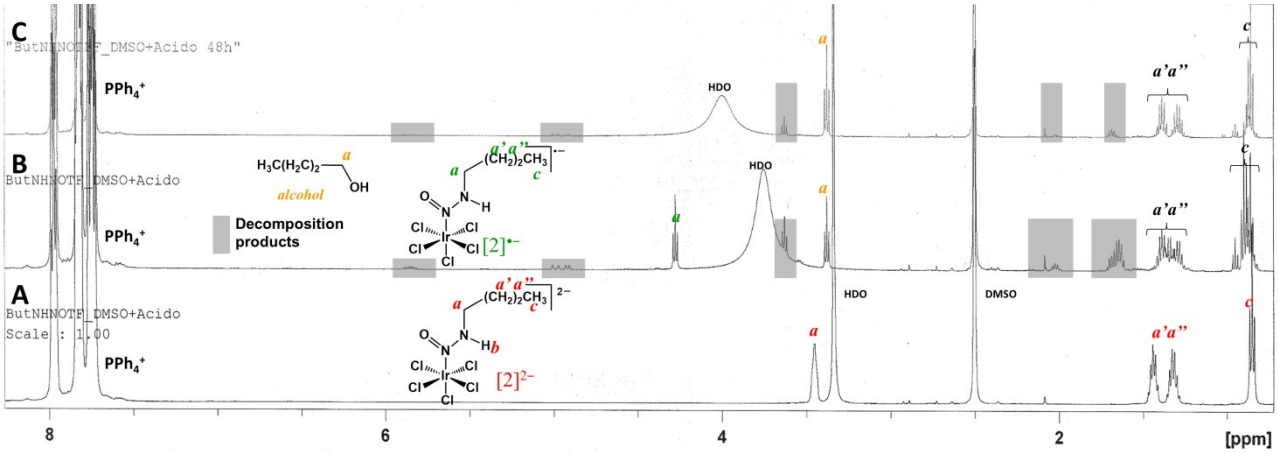

Figure S7. Decomposition of $(PPh_4)_2$[**2**] in DMSO-d^6/TFA (trifluoroacetic acid) followed by ^{1}H NMR (500 MHz) spectroscopy. **A**: starting complex**. B**: spectrum recorded immediately after addition of 1 equivalent of TFA. At 4.4 ppm butyl alcohol is detected, other yet un-identified decomposition products are highlighted in grey. **C**: spectrum recorded after 48 h.

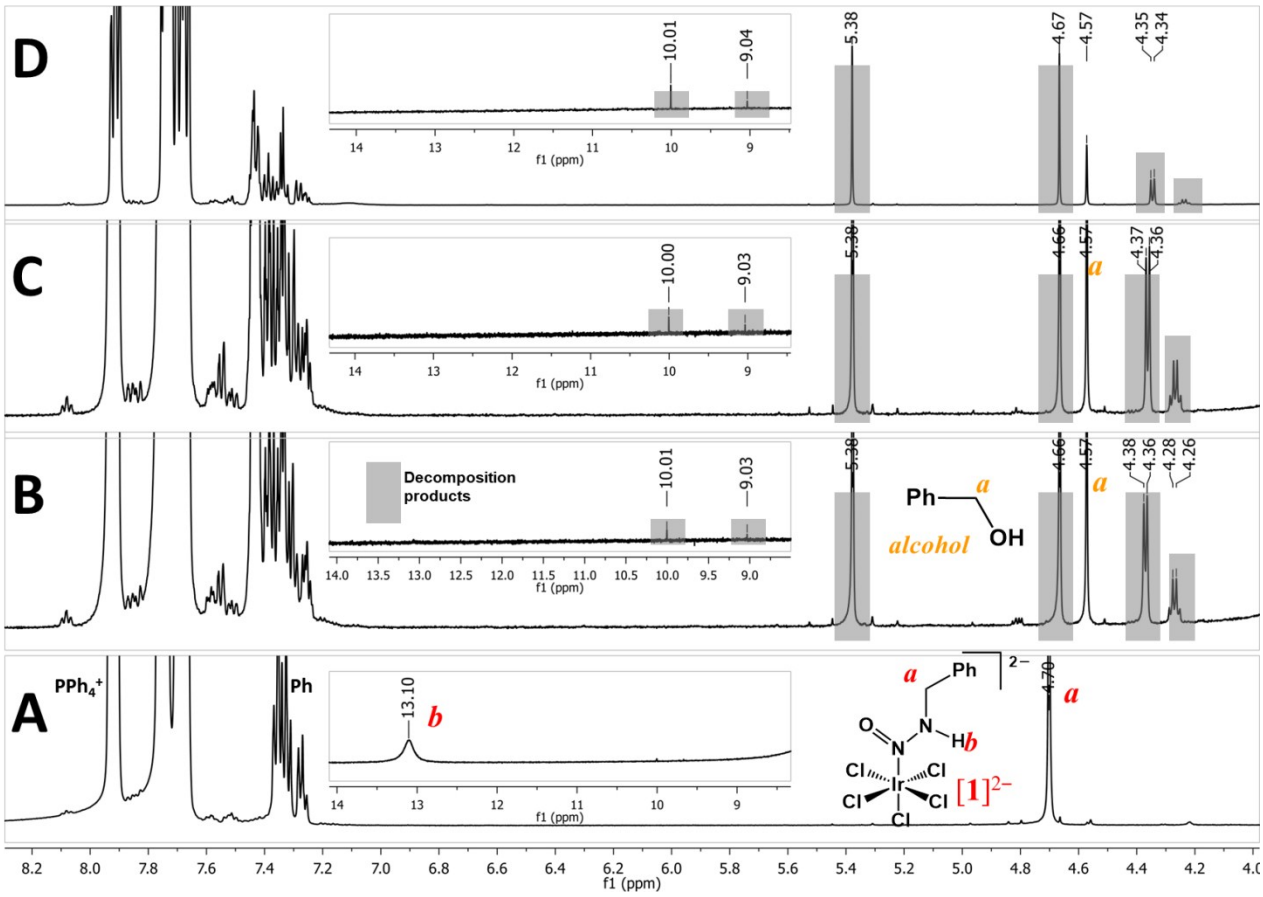

Figure S8. Decomposition of $(PPh_4)_2$[**1**] in MeCN-d^3/TFA (trifluoroacetic acid) followed by ^{1}H NMR (500 MHz) spectroscopy. **A**: starting complex. **B**: spectrum recorded immediately after addition of 1 equivalent of TFA. The species observed at 4.57 ppm can be assigned to benzylalcohol; **C**: spectrum recorded after 50 min. **D**: spectrum recorded after 2 h.

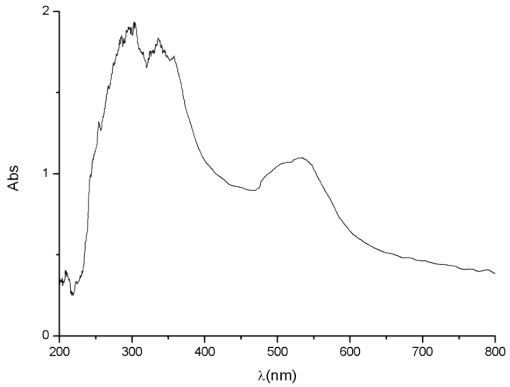

Figure S9. UV-vis absorption spectrum of isolated solid (PPh_4)[**1**] dissolved in MeOH.

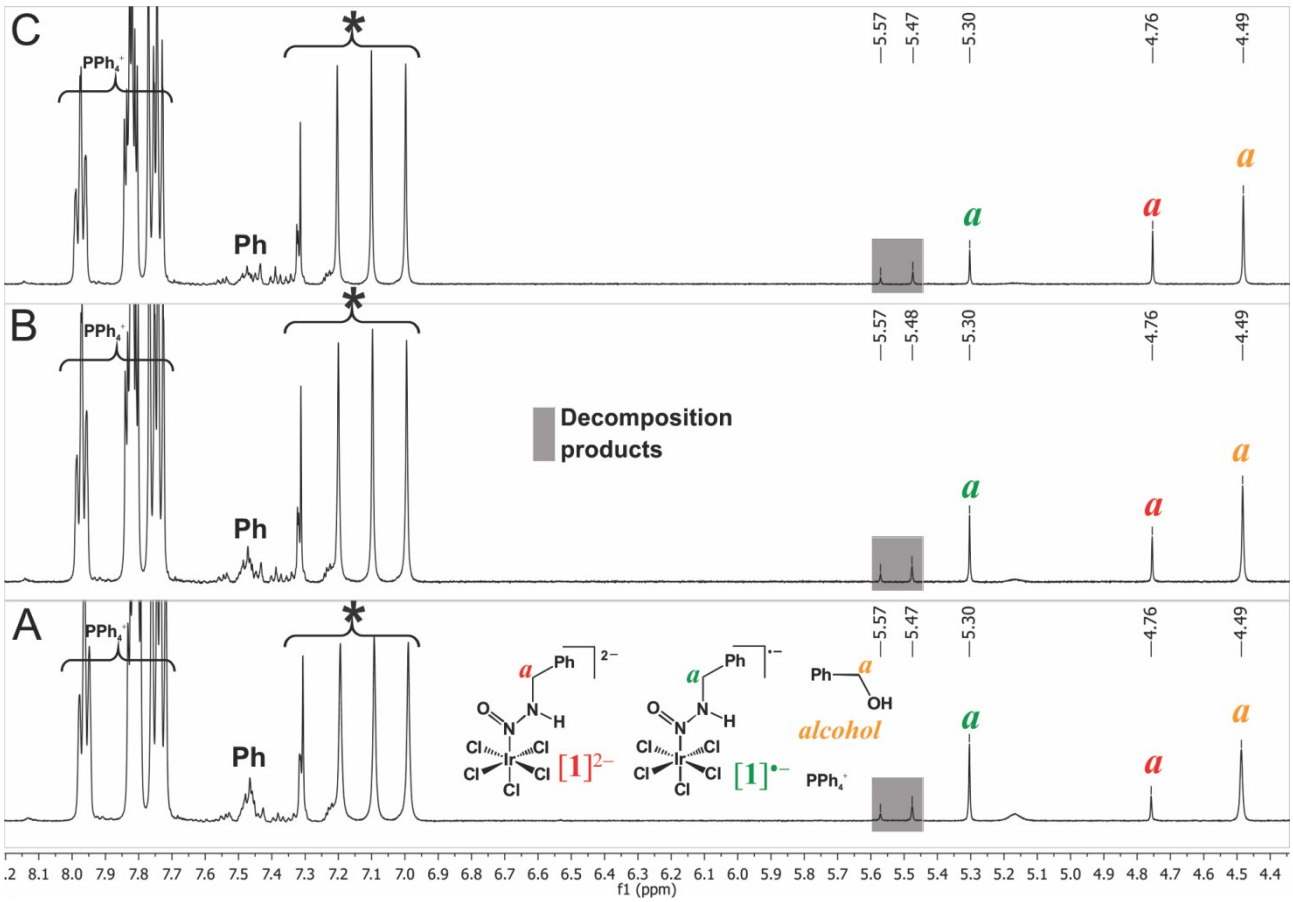

Figure. S10 ^{1}H NMR (500 MHz) spectra of isolated (PPh_4)[**1**] dissolved in DMSO-d^6. **A**: spectrum recorded immediately after dissolution. **B**: spectrum recorded after 10 minutes. **C**: spectrum recorded after 30 minutes. NH_4^+ protons of the $Ce^{III/IV}$ complexes impurities are indicated with *.

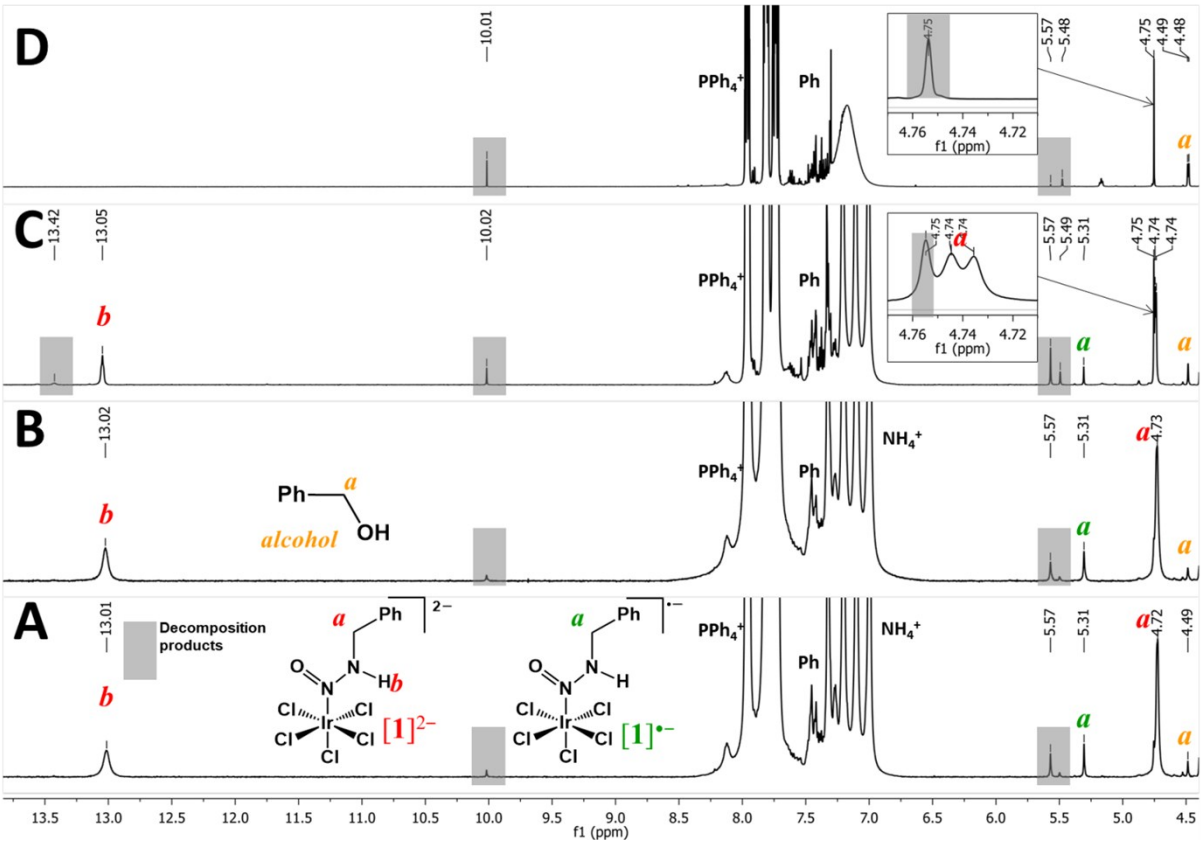

Figure S11. ^{1}H NMR (500 MHz) spectra of isolated (PPh_4)[**1**] dissolved in DMSO-d^6 at higher concentration than experiment showed in Figure S9. **A**: spectrum recorded immediately after dissolution; **B**: spectrum recorded after 10 minutes; **C**: spectrum recorded after 30 minutes; **D**: spectrum recorded after 3 days. The signal [**1**]$^{\bullet-}$ has completely vanished, benzyl alcohol is the main product.

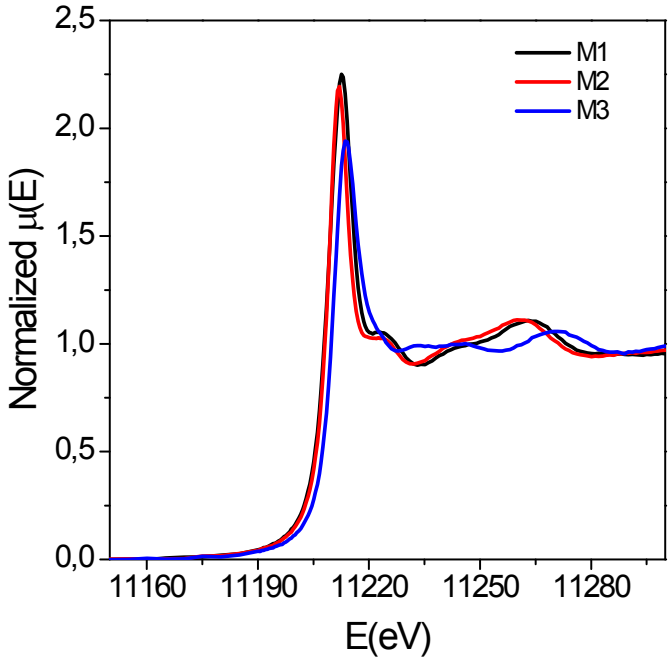

Figure S12. Normalized XANES spectra at the Ir L_3 edge for the reference samples. **M1**: $K_2[Ir^{IV}Cl_6]$, **M2**: $K_3[Ir^{III}Cl_6]$, **M3**: $K[Ir^{I}Cl_2(CO)_2]$. The displacement of the absorption edge observed for **M3** is attributed to the different surrounding than **M1** and **M2**, as expected.

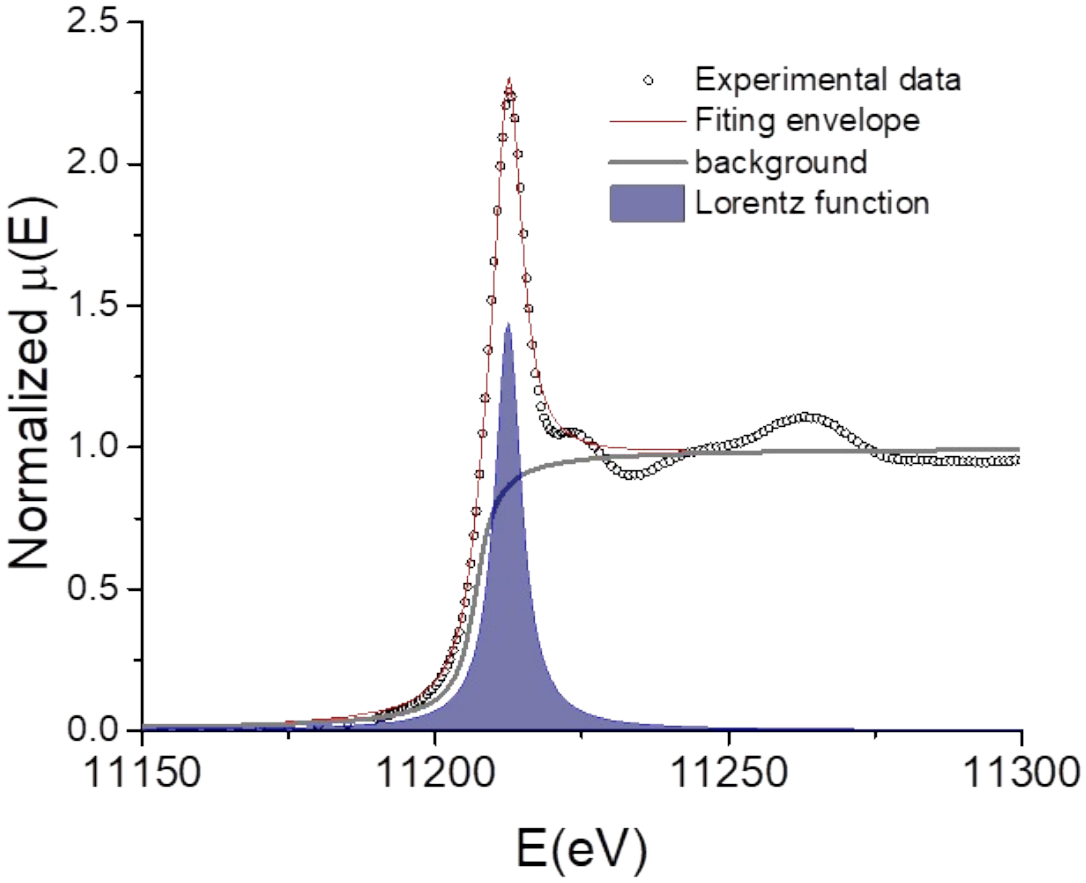

Figure S13. Lorentzian function employed to fit the white-line intensity to perform the calibration procedure.

C Supporting information on the XANES measurements

Sometimes the variation in the oxidation state results in a smaller energy shift than the intrinsic energy uncertainty at the corresponding electronic level, so this methodology is not sensitive enough to determine the energy shift and the only parameter suitable for determination of the oxidation state is the intensity of the white line. Moreover, when the nature of the moieties surrounding the absorbing atoms differs among samples, the shift is not an unequivocal parameter since the total energy shift comprises an intricate superposition of factors (for example, geometry, orbital hybridization, charge transfer).[S5,S6] Like the L_3 white lines, the L_2 white lines for Ir are attributed to transitions from 2p orbitals to partially occupied bands at the Fermi level with a largely 5d character. Since precisely d electrons are involved in Ir–Cl or Ir–N bonds, the L_2- and L_3-edge XANES spectra will be particularly sensitive to changes in redox state. L_2 and L_3 are associated with the dipole allowed electronic transitions $2p_{1/2} \rightarrow 5d_{3/2}$ and $2p_{3/2} \rightarrow 5d_{5/2}$ respectively, but the increment at the L_3 white line does not necessarily imply that L_2 should also increase, because the overlapping differs at the $5d_{5/2}$ and $5d_{3/2}$ levels of Ir in the molecule. Moreover, the constant intensity of the L_2 white line indicates that the increment originates mainly in variations in the occupancy at the $5d_{5/2}$ level.

Figure S12 shows the normalised L_3 XANES spectra of the Ir reference samples **M1**: $K_2[Ir^{IV}Cl_6]$, **M2**: $K_3[Ir^{III}Cl_6]$, and **M3**: $K[Ir^{I}Cl_2(CO)_2]$. The variations of the white line intensities are related to

the oxidation state numbers. In order to quantify those visible changes, the areas of the white lines were determined by a non-lineal fitting routine using the WinSAS2000 software[S7] with two functions: an *arctan* function for the background and a Lorentzian function for the white line (Figure S13).

D. References

S1. L. Moggi, G. Varani, M. F. Manfrin, V. Balzani, *Inorg. Chim. Acta*, 1970, **4**, 335–341.
S2. a) C. K. Jorgensen, *Mol. Phys.*, 1959, **2**, 309–332. b) C. K. Jorgensen, *Acta Chem. Scand.* 1956, **10**, 500–517.
S3. M. J. Davies, T: F. Slater, *Chem.-Biol. Interact.* 1986, ***58***, 137–147.
S4. (a) L. Eberson, O. Persson, *J. Chem. Soc., Perkin Trans. 2* 1997, 893-898. (b) L. Eberson, O. Persson, *J. Chem. Soc., Perkin Trans. 2* 1997, 1689–1696.
S5. J. L. DuBois, P. Mukherjee, T. D. P. Stack, B. Hedman, E. I. Solomon and K. O. Hodgson, *J. Am. Chem. Soc*., 2000, **122**, 5775 –5787.
S6. T. E. Westre, P. Kennepohl, J. G. DeWitt, B. Hedman, K. O. Hodgson and E. I. Solomon, *J. Am. Chem. Soc.* 1997, **119**, 6297 –6314.
S7. T. Ressler. WinXAS: A new Software package not only for analysis of energy-dispersive XAS data. *J. Physique IV*, 1997, **7**, 269–270.